Petroleum Science 19 (2022) 2314–2325

Contents lists available at ScienceDirect

Petroleum Science

journal homepage: www.keaipublishing.com/en/journals/petroleum-science

Original Paper

Solidification and utilization of water-based drill cuttings to prepare ceramsite proppant with low-density and high performance

Hang Yang [a], Yun-Li Liu [b], Guo-Liang Bai [b], Zhen Feng [a], Yi Zhang [b, **], Shi-Bin Xia [a, *]

[a] School of Resources and Environmental Engineering, Wuhan University of Technology, Wuhan, 430070, Hubei, PR China
[b] State Key Laboratory of Freshwater Ecology and Biotechnology, Institute of Hydrobiology, Chinese Academy of Sciences, Wuhan, 430072, Hubei, PR China

ARTICLE INFO

Article history:
Received 12 September 2021
Received in revised form
10 June 2022
Accepted 12 June 2022
Available online 15 June 2022

Edited by Yan-Hua Sun

Keywords:
Water-based drill cuttings
Proppant
Thermal analysis
Solid waste

ABSTRACT

Water-based drill cuttings (WBDC) and bauxite are used as raw materials to prepare proppants with low density and high performance. The effects of sintering temperature, sintering period, mixture ratios of materials, doping with iron oxide, and acid modification of WBDC on the properties of proppants are discussed. The proppant performance is evaluated according to the national standard SY/T5108-2014. The morphology of the proppant is analyzed using scanning electron microscopy (SEM). The crystal phase structure of the proppant is studied using X-ray diffraction (XRD). Thermal analysis of the proppant sintering process is performed using thermogravimetry (TG). Proppant Z-23 completely satisfied the SY/T5108 -2014 standard. This study provides a new perspective for the resource utilization of water-based drill cuttings and preparation of low-density proppants.

1. Introduction

Water-based drilling cuttings (WBDC) are main solid waste produced in the process of shale gas drilling (Liu et al., 2018). Usually, WBDC are soaked in by water-based drilling fluid and carried to the ground by drilling fluid, resulting in a complex composition of WBDC (Pang et al., 2019). The direct discharge of WBDC causes pollution of environment and ecosystems (Nguyen et al., 2021). Therefore, the rational treatment and utilization of WBDC has important significance for sustainable development of shale gas industry.

Currently, the common treatment method for WBDC is to directly deposit them into a soil or marine landfill. Thus, they occupy a large amount of land and poses potential secondary environmental risks (Kogbara et al., 2016, 2017; Leonard and Stegemann, 2010). Through the solidification process, the dominant contaminants found in WBDC are blended into the solidified blocks (Kogbara et al., 2016). It is necessary to develop green, fast, safe, and environmentally friendly disposal methods for WBDC. Resource utilization is an important method for WBDC treatment. Currently, WBDC is employed as a raw source for the preparation of industrial and building materials (Khodadadi et al., 2020; Wang and Xiong, 2021; Yang et al., 2020). Wang et al. studied the co-processing of WBDC and phosphogypsum for the preparation of non-autoclaved aerated concrete (Wang C.-q. et al., 2020), which could fully meet the $A_{3.5}$ grade of China State Standard (GB/T11968-2006) without secondary contamination. Liu et al. used WBDC as a replacement for natural clay to prepare sintered bricks, which met the requirements of the corresponding Chinese and ASTM standards (Liu et al., 2021). Liu et al. used WBDC with other cementitious materials to prepare non-fired bricks that met grade M10 according to Chinese standard (GB/T2542-2012) (Liu et al., 2018). Owing to the larger number of WBDC produced (300000 tons annually in China), it is necessary to develop new feasible resource utilization methods.

In China, the exploration of oil and gas resources is thriving. To increase exploitation, hydraulic fracturing technology is widely used to utilize oil and gas resources (Hao et al., 2019; Thomas et al., 2019). Ceramsite proppant is a key material in the hydraulic fracturing of oil and gas wells (Wang J. et al., 2020, Xu et al., 2019; Zhang et al., 2017). Bauxite is a common material for proppant preparation because of its widespread availability and low cost. However, density and other performance factors are important limiting factors for proppants. Furthermore, proppants prepared

* Corresponding author.
** Corresponding author.
E-mail addresses: zhangyi@ihb.ac.cn (Y. Zhang), xiashibin@126.com (S.-B. Xia).

https://doi.org/10.1016/j.petsci.2022.06.006

using pure bauxite do not meet this requirement (Hao et al., 2018b; Ma et al., 2016; Yang et al., 2016). To solve this problem, other materials and extra additions have been used to prepare proppants with low density and high performance. The chemical composition of WBDC includes many metal components such as calcium oxide, barium oxide, and iron oxide. Research indicates that the addition of calcium oxide could decrease the sintering temperature of the proppants (Hao et al., 2018b; Liu et al., 2016), whereas the addition of barium oxide in the proppant reduced the acid solubility (Han et al., 2018; Wu et al., 2013). Moreover, the addition of iron oxide could also enhance the breakage resistance of the proppant (Abd El-Kader et al., 2020; Han et al., 2018). Therefore, WBDC could theoretically be employed as a raw material for the preparation of proppants. At present, proppants are produced on an industrial scale in China. Using WBDC as a raw material to replace certain amount of bauxite not only reduces the material cost but also realizes the resource utilization of WBDC, which is an economical and feasible developmental approach (Li et al., 2018; Yao et al., 2022). For this purpose, we explored the use of WBDC for proppant preparation.

The aim of this study is to use WBDC as a raw material for the preparation of low-density proppants, which not only realizes the resource utilization of WBDC but also increases oil and gas field production. The performance of the prepared proppant was tested using specific indices. In addition, acid modification of WBDC and the addition of metal oxides were employed to enhance the performance index of the prepared proppant. The morphology and structural phase of the proppant were analyzed using scanning electron microscopy (SEM) and X-ray diffraction (XRD), respectively. The thermal characterization of the proppant sintering process was performed using thermogravimetry (TG).

2. Materials and methods

2.1. Materials and instruments

Bauxite was purchased from Gongyi Wanying Environmental Protection Material Co. Ltd. WBDC was provided by the Fuling Shale Gas Company. Manganese powder (MnO_2) was purchased from Sinopharm Chemical Reagent Co. Ltd. The physical and chemical properties of WBDC and bauxite were analyzed using inductively coupled plasma optical emission spectroscopy (ICP-OES), XRD, C/H/N/S/O element analysis, and X-ray fluorescence (XRF) (The results are shown in Tables S1–S6 and Figs. S1–S2 in Electronic Supplementary Material).

A disc granulator (PQ-10) was used to prepare the proppant precursors. An X-ray photoelectron spectrum analyzer (XPS, ESCALAB 250Xi) was used to determine the surface compositions of the samples. An X-ray diffractometer (Empyrean) was also used to record the XRD data. A field-emission SEM (JSM-IT300) was used to observe the morphology of the samples. An ICP-OES (ICP, Prodigy 7) was employed to test the chemical components of the material. A camera (Canon) was used to photograph the samples and determine their roundness and sphericity. An XRF (XRF-1800) was used to investigate the chemical compositions of the samples. A scattering turbidity meter (Xipu TU-1810) was used to measure the turbidity of the leachate. Fragmentation rate tests were performed using a pressure-testing machine (YAW-300). Bulk and visual density were measured using a bulk density meter and precision density bottle, respectively. A C/H/N/S/O element analyzer was employed to detect the elements in the sample (Vario EL cube). The oil content was measured using an infrared spectrophotometer (SYT700), and a synchronous thermal analyzer (STA449F3) was used to analyze the thermodynamic process.

2.2. Drying of WBDC and acid modification for WBDC

Raw WBDC was washed five times using pure water to remove soluble impurities, and then the WBDC was filtered out using gauze. 2000 g treated WBDC was evenly and thinly placed in a tray and then dried in a dryer at 105 °C for 24 h.

Dried WBDC (100.0 g) was added to a 1000 mL beaker including 300 mL of pure water. A certain amount of hydrochloric acid (6 mol/L) was then slowly added to the beaker, and the WBDC was soaked for 24 h. The acid treated WBDC was filtered with a suction filter and rinsed with pure water until the solution was neutral. The obtained WBDC was dried again in a dryer at 105 °C for 24 h.

2.3. Preparation procedure of proppant

The proppant was prepared by the disc granulation method. A mixture of bauxite, WBDC, and manganese powder at different ratios were added to the disc granulation machine. The proppant precursor was prepared by spraying a shower and passing it through a 20–40 mesh sieve. The sieved proppant precursor was placed in a crucible and sintered in a muffle furnace for different time periods. The sintered proppant was cooled in the atmosphere and sieved again through a 20–40 mesh sieve. The formula for the proppant is shown in Table 1, and the XRF data of each sample were tested, as listed in Table S7 in Electronic Supplementary Material. The addition of iron oxide (Z17–Z20) and acid modification of WBDC (Z21–Z25) was further investigated to enhance the performance of the proppant to meet the SY/T5108-2014 standard. The corresponding formula is shown in Tables 2 and 3, and the XRF data of each sample were tested, as shown in Tables S8 and S9 in Electronic Supplementary Material.

2.4. Proppant performance test

The turbidity, acid solubility, bulk density, apparent density, roundness, sphericity, and breakage ratio of the proppant were tested according to the oil and gas industry standard SY/T5108-2014 (Hao et al., 2018a; Tang et al., 2017).

3. Results and discussion

3.1. Performance test of proppant

Performance testing of the proppant is important for determining the optimal preparation parameters. The turbidity, acid

Table 1
Formula for preparation of proppant samples Z-1– Z-16.

Code	Content of raw material, g		
	Bauxite	WBDC	Manganese powder
Z-1	190	10	0
Z-2	180	20	0
Z-3	160	40	0
Z-4	140	60	0
Z-5	190	10	4
Z-6	180	20	4
Z-7	160	40	4
Z-8	140	60	4
Z-9	190	10	8
Z-10	180	20	8
Z-11	160	40	8
Z-12	140	60	8
Z-13	190	10	12
Z-14	180	20	12
Z-15	160	40	12
Z-16	140	60	12

Table 2
Formula for preparation of proppant samples Z-17–Z-20.

Code	Content of raw material, g				Sintering temperature, °C	Sintering time, h
	Bauxite	WBDC	Manganese powder	Iron oxide		
Z-17	140	60	8	4	1420	2.0
Z-18	140	60	8	6	1420	2.0
Z-19	140	60	8	8	1420	2.0
Z-20	140	60	8	10	1420	2.0

Table 3
Formula for preparation of proppant samples Z-21–Z-25.

Code	Pretreatment of WBDC	Content of raw material, g				Sintering temperature, °C	Sintering time, h
	Amount of hydrochloric acid, mL	Bauxite	WBDC	Manganese powder	Iron oxide		
Z-21	20	140	60	8	4	1420	2.0
Z-22	60	140	60	8	4	1420	2.0
Z-23	100	140	60	8	4	1420	2.0
Z-24	120	140	60	8	4	1420	2.0
Z-25	140	140	60	8	4	1420	2.0

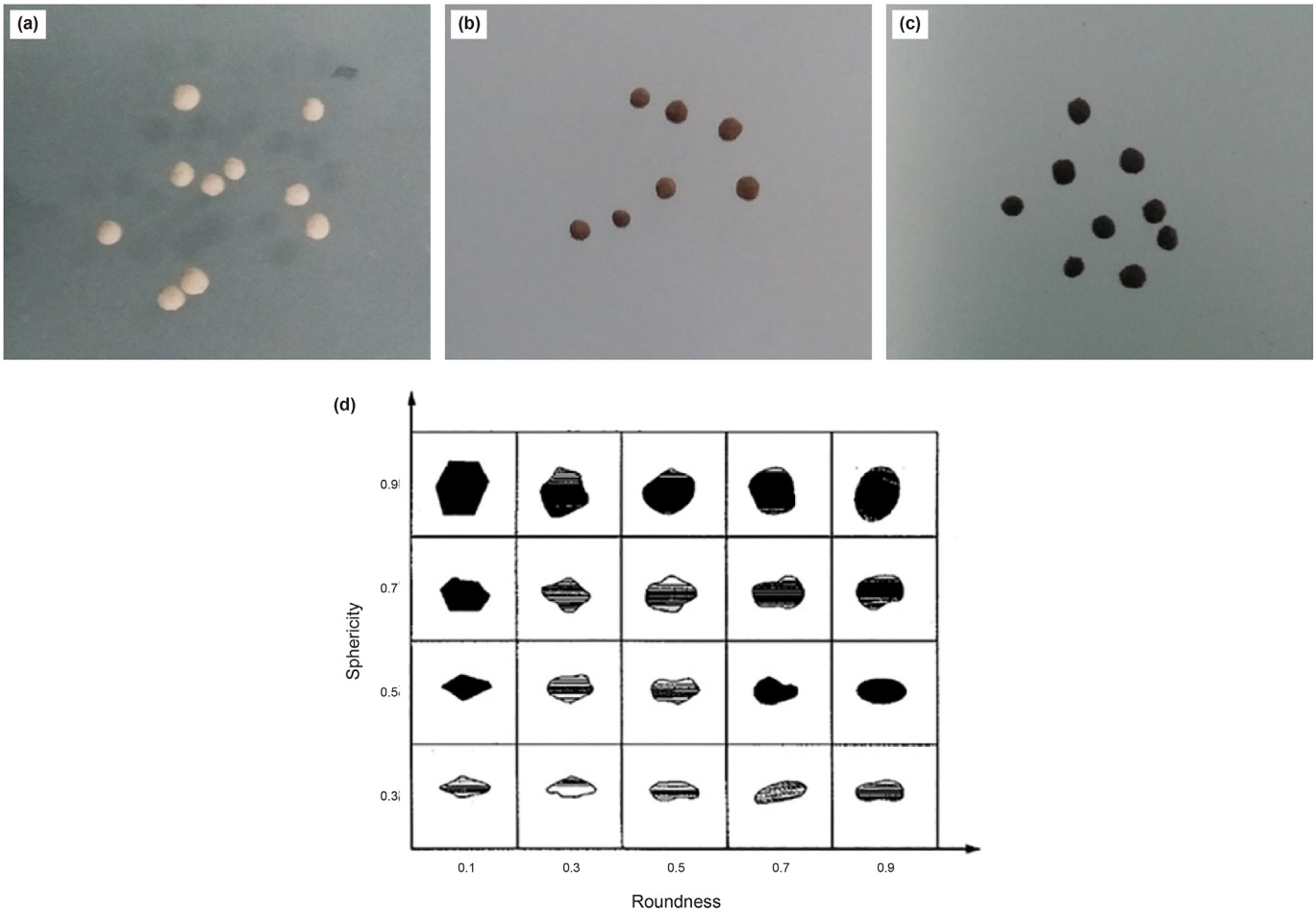

Fig. 1. Photographs of the three groups of proppant samples: (**a**) Z-2, (**b**) Z-7, (**c**) Z-13, and (**d**) Krumbien/Sloss template.

solubility, bulk density, apparent density, roundness, sphericity, and breakage ratio were used as indices to evaluate the performance of the proppant.

The Krumbien/Sloss template was used to check roundness and sphericity. Three photographs of the proppant samples were selected, which are shown in Fig. 1. The average roundness and sphericity of all samples (Z1–Z25) were above 0.8. All meet the requirements of roundness and sphericity: greater than or equal to 0.7 provided in the oil and gas industry standard SY/T5108-2014.

Oil and gas field production is affected by proppant turbidity. With the increasing turbidity of the proppant, the pores between the proppants are more easily blocked, which results in reduced

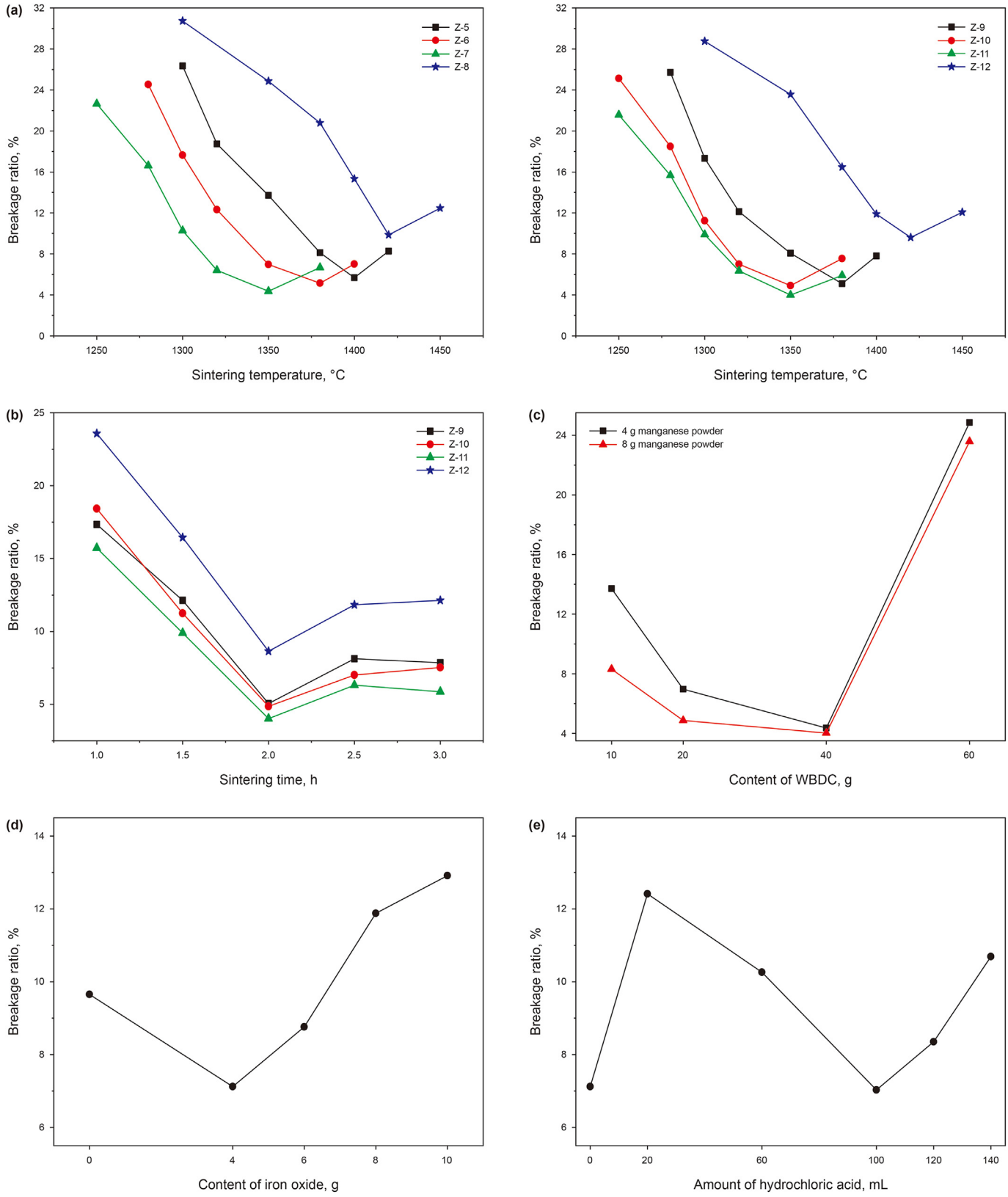

Fig. 2. The breakage ratio of the proppant with different preparation parameters: (**a**) sintering at different temperatures for 2 h for Z-5 to Z-12, (**b**) sintering for different times at 1350 °C for Z-9 to Z-12, (**c**) different contents of WBDC with the addition of manganese power at 1350 °C for 2 h for Z-5 to Z-12, (**d**) different contents of iron oxide for Z-17 to Z-20 at 1420 °C for 2 h, and (**e**) different amounts of hydrochloric acid for Z-21 to Z-25 at 1420 °C for 2 h.

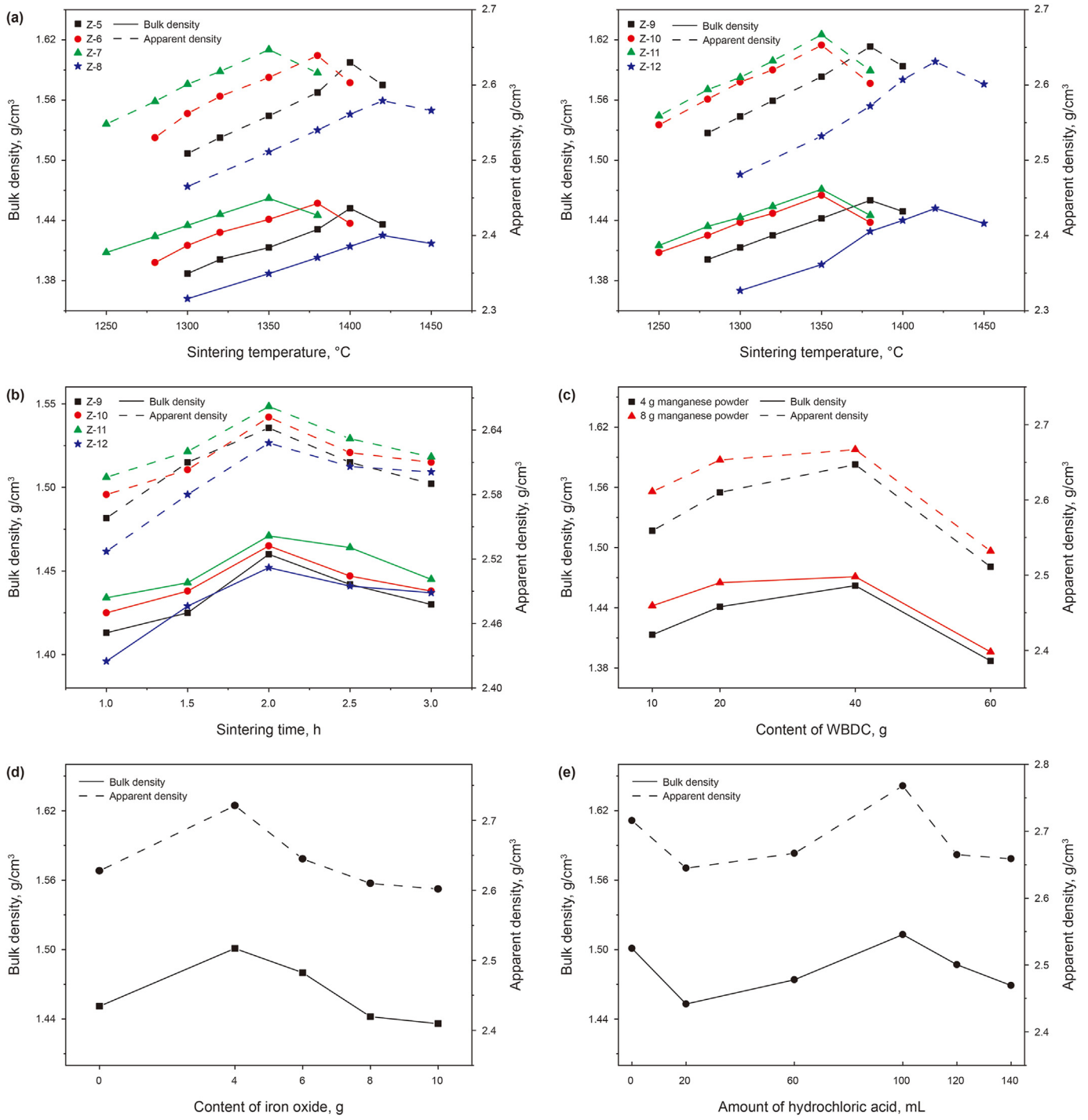

Fig. 3. The bulk density and apparent density of the proppant with different preparation parameters: (**a**) sintering at different temperatures for 2 h for Z-5 to Z-12, (**b**) sintering for different lengths of time at 1350 °C for 2 h for Z-9 to Z-12, (**c**) different contents of WBDC at 1350 °C for 2 h for Z-5 to Z-12, (**d**) different contents of iron oxide for Z-17 to Z-20 at 1420 °C for 2 h, and (**e**) different amounts of hydrochloric acid for Z-21 to Z-25 at 1420 °C for 2 h.

conductivity of the proppant. Table S10 in Electronic Supplementary Material lists the turbidity of the proppant. The turbidity of all proppant samples was between 10 and 20 NTU, which meets the standard SY/T5108-2014 standard (<100 NTU).

Acid solubility was used to characterize the acid resistance of the proppant. A lower acid solubility is beneficial for increasing the service life of the proppants (Han et al., 2018). Tables S11–S13 in Electronic Supplementary Material show the acid solubilities of the proppant. The acid solubility of most proppant samples in Z-1–Z-16 was above 7.0%, which does not meet the SY/T5108-2014 standard (<7.0%). Among all the samples, sample Z-11, sintered at 1380 °C for 2 h, exhibited the lowest acid solubility of 6.72%. The presence of a large amount of alkaline earth metal oxides in WBDC, such as calcium and magnesium oxide, promotes the formation of anorthite and glass phases in the proppant, resulting in relatively high acid solubility. High acid solubility usually appears with the addition of iron oxide, which promotes the formation of liquid and glass phases during the sintering process. In addition, due to the

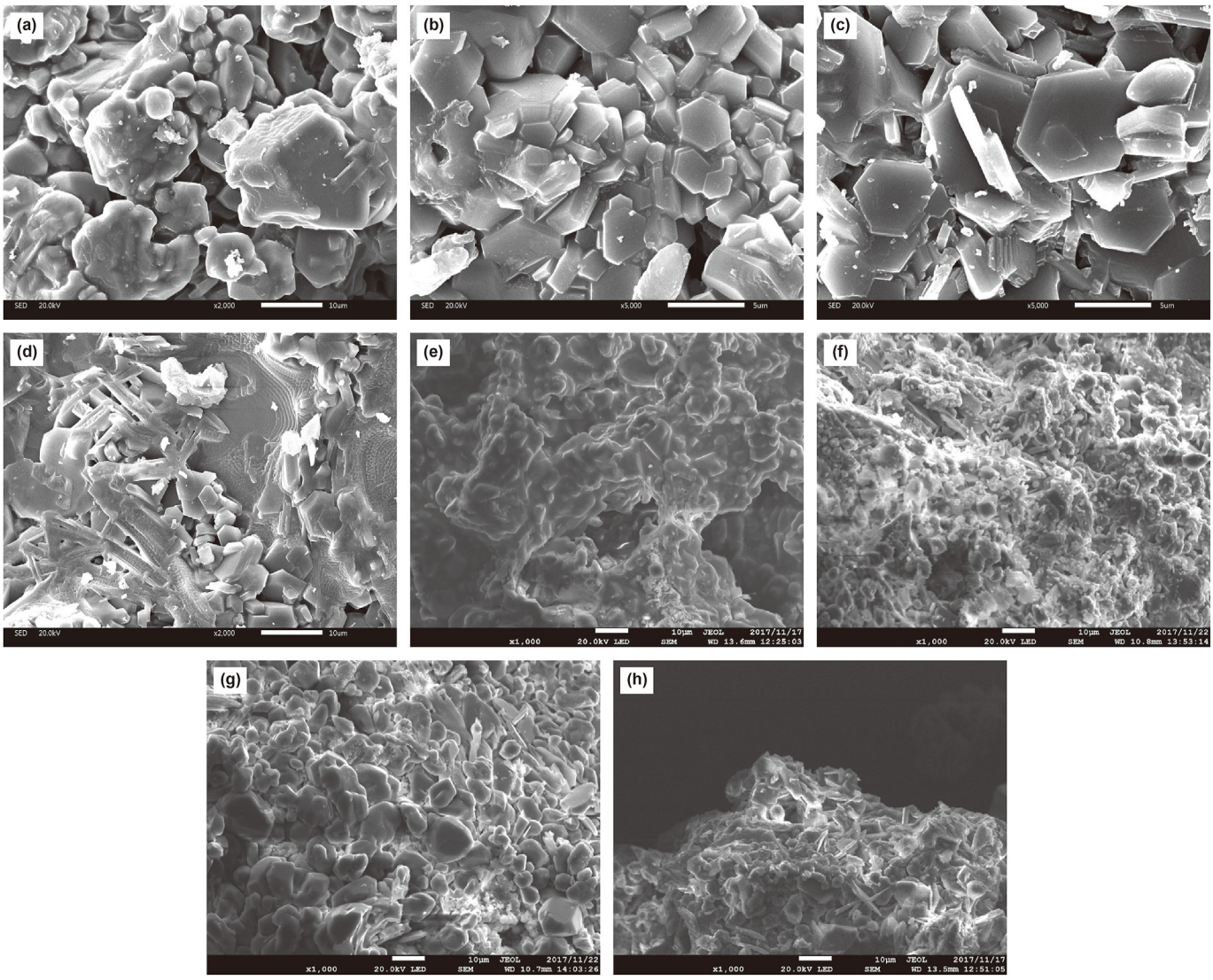

Fig. 4. SEM images of sample Z-12 sintered at different temperatures for 2 h: (**a**) 1300 °C, (**b**) 1320 °C, (**c**) 1350 °C, and (**d**) 1380 °C; SEM images of proppants sintered at 1350 °C for 2 h with different WDC contents: (**e**) Z-9, (**f**) Z-10, (**g**) Z-11, and (**h**) Z-12.

high acid solubility and high catalytic activity of manganese powder, the excessive addition of manganese powder could also contribute to the high acid solubility. Acid treatment was conducive to reducing the acid solubility of the sample owing to the reduction in the content of alkaline earth metal oxides in WBDC.

A low breakage ratio, bulk density, and apparent density are beneficial for enhancing the proppant conductivity, resulting in a high production of oil and gas fields (Xie et al., 2019). Figs. 2 and 3 show the effects of these parameters on the breakage ratio and density, respectively. For the proppant without iron oxide addition and acid modification, when the sintering temperature and time increased, the breakage ratio of the proppant decreased and increased, respectively; meanwhile, the bulk density and apparent density of the proppant increased and decreased, respectively. Other parameters exhibited similar effects on the breakage ratio and density of the proppant. The breakage ratio is inversely proportional to the bulk and apparent densities. Based on a comprehensive consideration of the performance of proppant samples Z-1–Z-16, it was found that the preparation scheme used for proppant sample Z-12 was optimal, i.e., sintered at 1420 °C for 2 h.

However, the acid solubility and breakage ratio of proppant Z-12 are undesirable. To improve these properties, the addition of iron oxide (to decrease the breakage ratio) and acid modification of WBDC (to decrease acid solubility) were used based on the formula (ratio of raw material) of proppant Z-12. For the proppants that have undergone iron oxide addition (Z-17–Z-20), an obvious decrease in the breakage ratio was observed, while the acid solubility increased. Therefore, further acid treatment of WBDC is required. For the proppants with iron oxide addition and acid modification (Z-21–Z-25), the acid solubility for proppant samples Z-22–Z-25 met the SY/T5108-2014 standard. Based on a comprehensive consideration of the performance of proppant samples Z-17–Z-25, the preparation parameter used for proppant Z-23 was identified as optimal—sintered at 1420 °C for 2 h.

3.2. Morphology analysis

Figs. 4 and 5 show SEM images of the proppant samples prepared under different conditions. Corundum belongs to the trigonal crystal system, and the crystal exhibits a hexagonal columnar shape. Multiple corundum grains are gathered to form a granular shape. Corundum has the advantages of high hardness, strength,

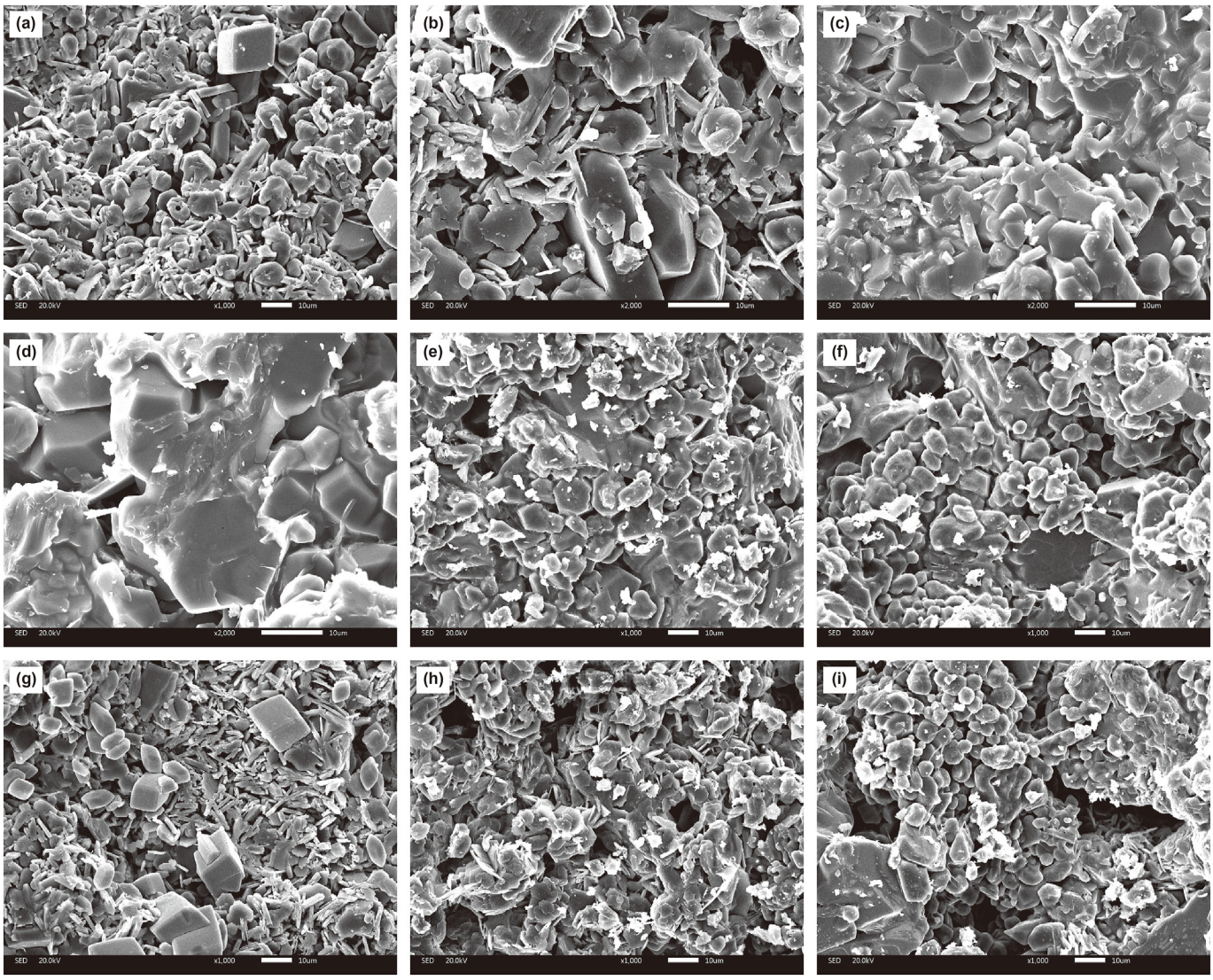

Fig. 5. SEM images of samples sintered at 1420 °C to which different contents of Fe_2O_3 are added: (**a**) Z-19, (**b**) Z-18, (**c**) Z-19, and (**d**) Z-20; SEM images of samples sintered at 1420 °C to which different amounts of acid are added: (**e**) Z-21, (**f**)Z-22, (**g**) Z-23, (**h**) Z-24, and (**i**) Z-25.

and resistance to chemical erosion (Chen et al., 2019). Mullite belongs to the orthorhombic crystal system, and the mullite grains are usually needle or rod-shaped (Liu et al., 2020). When the sintering temperature was 1300 °C, the proppant sample was mainly composed of small corundum grains with loose internal structures and pores. When the sintering temperature was increased to 1380 °C, the surface of the proppants exhibited an obvious cross structure of the corundum and mullite phases. Considering the content of WBDC, when the content of WBDC was 10 g, some holes exited on the smooth surface of the proppant. When the content of WBDC was increased to 60 g, the hole gradually disappeared and the surface became coarse. In the terms of the iron oxide addition, when the iron oxide addition was 4 g, large quantities of non-compact debris appeared on the surface of proppant. When 10 g of oxide was added, the compactness of the WBDC surface significantly improved owing to the sintering effect of the iron oxide (Kao et al., 2018). When 20 mL of HCl was added for modification, the surface of the crystal phase was covered with a layer of glass phase. There were also some irregular closed pores inside, which may be a positive effect caused by the increase in the relative content of the calcium ferrite and calcium aluminum ferrite phases. When 100 mL of HCl was added, the glass phase was essentially used to fill the pores between the solid phase crystal grains, resulting in good compactness of the structure. When the 140 mL HCl was added, some open pores were formed on the surface of the proppant, which seriously affected the compressive strength and density of the ceramsite proppant.

3.3. XRD pattern of proppant

Fig. 6 shows XRD patterns of the proppant samples with different preparation parameters. Corundum with high crystallinity can improve the compressive strength of the proppant (Deon et al., 2013), and a certain number of mullite grains can enhance the toughness of the ceramsite proppant, thereby reducing the breakage ratio of the sample (Abd El-Kader et al. 2020). When the sintering temperature was increased from 1300 to 1350 °C, the diffraction peak intensity of the corundum phase increased and the peak width narrowed, indicating that the relative content of the corundum phase and the crystallinity was improved. The diffraction peak of the mullite phase was weak, indicating that the relative content of the mullite phase was low. When the sintering

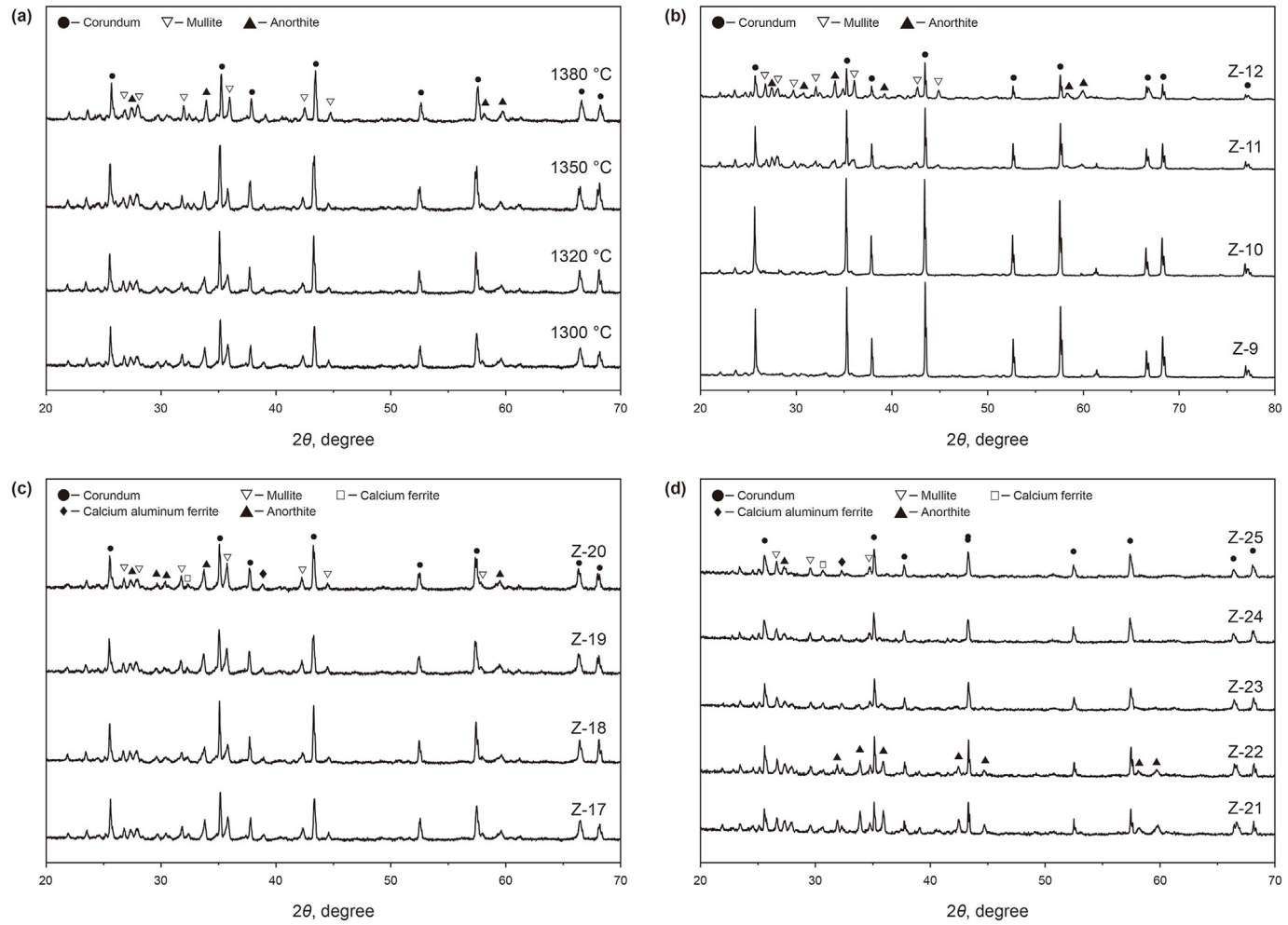

Fig. 6. XRD patterns of proppant samples: (**a**) Z-11 sintered at different temperatures for 2 h, (**b**) samples with different WBDC contents sintered at 1350 °C for 2 h, (**c**) samples sintered at 1420 °C with different contents of Fe_2O_3, and (**d**) samples sintered at 1420 °C with different amounts of hydrochloric acid.

temperature was not sufficiently high, it was difficult to form the mullite phase. When the temperature was increased from 1300 to 1350 °C, the peak intensity of the mullite phase increased. When the sintering temperature was increased from 1350 to 1380 °C, the diffraction peak intensities of the corundum and mullite phase both weakened to some extent. In addition, as the sintering temperature increased from 1300 to 1380 °C, the intensity of the anorthite phase diffraction peaks weakened, which may be caused by the reaction between the calcium oxide and silicon oxide in water-based drill cuttings and alumina in bauxite. Therefore, the anorthite phase gradually changed from the solid to liquid phase as the temperature increased.

The main crystalline phases of samples Z-9 to Z-12 were all corundum, which may be because the main component of the four groups of samples is alumina, with alumina contents of 70.69%, 67.14%, 60.14%, and 60.06%, respectively. When the WBDC content was low, the diffraction peak of the mullite phase in the sample was significantly weak, indicating that the crystallinity of the mullite phase was not obvious. This may be because the ratio of Al_2O_3/SiO_2 is large, which is highly conducive to the formation of the corundum phase. In addition, when a small content of WBDC was added, the intensity of the anorthite phase diffraction peak was extremely weak. This may be because the relative content of calcium oxide in the sample is low, which is not conducive to the reaction of calcium oxide with silicon aluminum oxide in the sample to form an anorthite phase. When 40 g WBDC was added, the intensity of the mullite phase diffraction peak in the sample significantly increased, while the corundum phase diffraction peak relatively weakened. This is because the Al_2O_3/SiO_2 ratio decreased with increasing WBDC content. Alumina and silica reacted easily to form a mullite phase. When the WBDC content was increased, the anorthite phase diffraction peaks increased, and the corundum and mullite phase diffraction peaks weakened. This may be due to the excessive addition of WBDC or excessive calcium oxide in the sample that reacts with alumina and silica to form anorthite, resulting in an increase in the relative content of anorthite, while reducing the corundum and mullite phases.

Corundum was the main crystalline phase for samples Z-17 to Z-20. This is because the main component of these samples is alumina, with alumina contents of 51.97%, 51.49%, 51.01%, and 50.54%, respectively. When 4 g of iron oxide was added, the diffraction peak of the mullite phase in the sample increased, indicating that the relative content of mullite in the sample and the crystallinity was high. A smaller Al_2O_3/SiO_2 ratio was conducive to the formation of the mullite phase. Simultaneously, the intensity of the anorthite phase diffraction peak was strong when more water-based drill cuttings were added because of the relatively large content of calcium oxide in the sample, which enabled the calcium oxide to react with alumina and silica to form an anorthite phase. With an increase in the iron oxide content, the diffraction peak

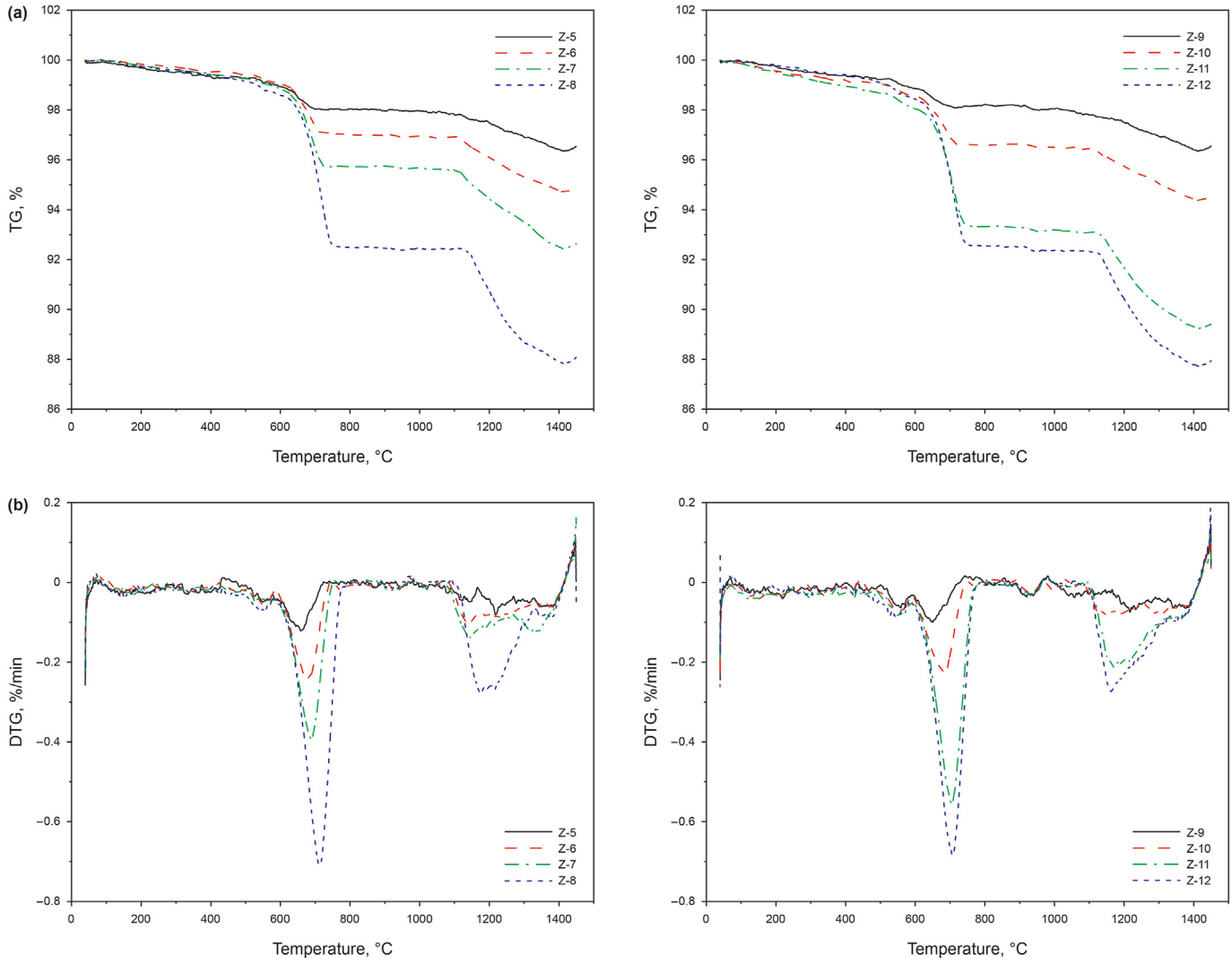

Fig. 7. TG (**a**) and DTG (**b**) curves of samples with different contents of WBDC.

intensity of the mullite phase in the sample increased, which was ascribed to the formation of the calcium ferrite phase and silicon calcium oxide due to the reaction of iron oxide and silicon calcium oxide. In addition, the calcium ferrite and calcium aluminate ferrite phases can be heated to easily form a liquid phase, which promoted diffusion and mass transfer, thereby increasing the relative content of the mullite phase.

The main crystalline phase of samples Z-21–Z-25 was corundum, and the diffraction peak intensity of the corundum phase showed no obvious differences, indicating that different volumes of acid treatment had little effect on the relative content of the corundum phase in the proppant sample. When 20 mL of hydrochloric acid was used to treat WBDC, the diffraction peaks of the anorthite phase in the sample were stronger, indicating that the relative content of anorthite in the sample and the crystallinity of the anorthite phase was high. This may be because the amount of hydrochloric acid added was too small, and the content of calcium oxide in the sample was still relatively large, which helped to form an anorthite phase. As the amount of hydrochloric acid for acid treatment increased, the intensities of the diffraction peaks of the anorthite phase in the sample decreased. When 100 mL of hydrochloric acid was added, the diffraction peaks of the anorthite phase disappeared, which may be due to the rapid reduction in the calcium oxide content in WBDC. In addition, as the amount of hydrochloric acid increased, the diffraction peak intensity of the mullite phase increased, which can be attributed to the low Al_2O_3/SiO_2 ratio; however, the diffraction peak intensities of the calcium ferrite and calcium aluminate ferrite phases increased and weakened consequently. This was owing to the addition of hydrochloric acid, which caused the reduced content of calcium oxide.

3.4. Thermal analysis

The sintering process was characterized using thermal analysis. Fig. 7 shows the TG and DTG curves of the proppant samples with different contents of WBDC. During the sintering of samples, two obvious weight-loss peaks appeared. Because the precipitation of water mainly occurs before the first weight loss peak, the increase in WBDC content had little effect on the TG and DTG curves of the first stage. The first weight loss peak appeared in the temperature range of 600–800 °C. As the WBDC content increased, the content of carbonate and other substances that are easily decomposed at high temperatures, especially calcium carbonate, increased, resulting in sample weight loss (Ren et al., 2019). The second weight loss peak appeared after 1000 °C. As the content of WBDC increased, the calcium oxide produced by decomposition increased,

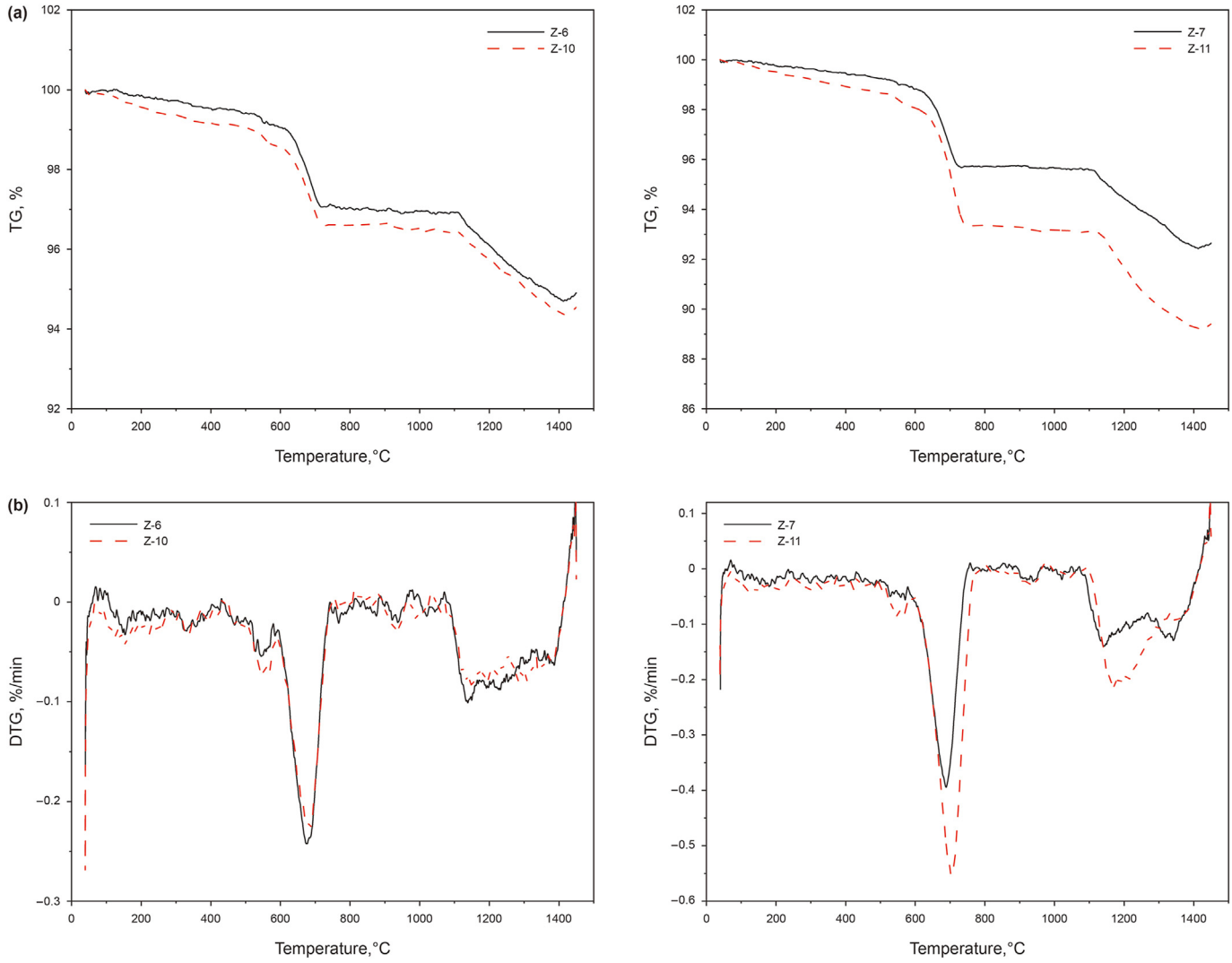

Fig. 8. TG (**a**) and DTG (**b**) curves of samples with different contents of manganese.

which contributed to the formation of the liquid phase, accelerated diffusion, and mass transfer, resulting in weight loss of the sample.

The effect of the manganese powder content on TG and DTG is shown in Fig. 8. The first weight loss peak appeared in the temperature range of 600–800 °C. An increase in the content of manganese powder (as a sintering aid) increased the weight loss rate of the sample. This may be because manganese oxide acts as a catalyst to accelerate the decomposition of carbonate in the raw material. Therefore, the greater the content of WBDC, the more obvious the changes in the TG and DTG curves. When the second weight loss peak appeared, the increase in the content of manganese powder was conducive to the transformation of the anorthite phase to the liquid phase, which promoted diffusion and mass transfer between the solid phase grains, resulting in fast sample weight loss and high weight loss rate.

The effect of the acid treatment amount on TG is shown in Fig. 9. The first weight loss peak appeared in the temperature range of 600–800 °C. With an increase in acid content, the decomposition reaction of the carbonate in WBDC decreased, resulting in a decrease in the sample's weight loss rate and a shift in the weight loss peak. When the second weight loss peak appeared, the increase in the amount of acid reduced the calcium oxide content in the sample, which was not conducive to the formation of the anorthite and liquid phases and hindered the diffusion and mass transfer between the solid phase grains, resulting in a low weight loss rate.

From the above analysis, it can be observed that samples Z-11 and Z-23 exhibited better performance. Therefore, the weight loss during the sintering of these two samples was analyzed. The TG, DTG, and DSC curves of samples Z-11 and Z-23 are shown in Fig. 10.

Two obvious weight loss peaks appeared during the sintering process of sample Z-11. Combined with TG curve analysis, the sintering process was divided into three stages. The first stage appeared before the first weight loss, and the TG curve showed a slow downward trend, which was due to the precipitation of free water and crystal water in the raw materials. The second stage appeared at 600–800 °C with an obvious weight loss peak, and the TG curve declined rapidly; this was due to the precipitation of the remaining moisture in the sample and oxidization and decomposition of organic matter, carbonate, and other substances. The third stage appeared at 1000–1400 °C with an obvious weight loss peak. In addition to decomposition and oxidation reactions, complex crystal phase transitions occurred. Additionally, the DSC curve indicated that the sintering of the proppant was an endothermic

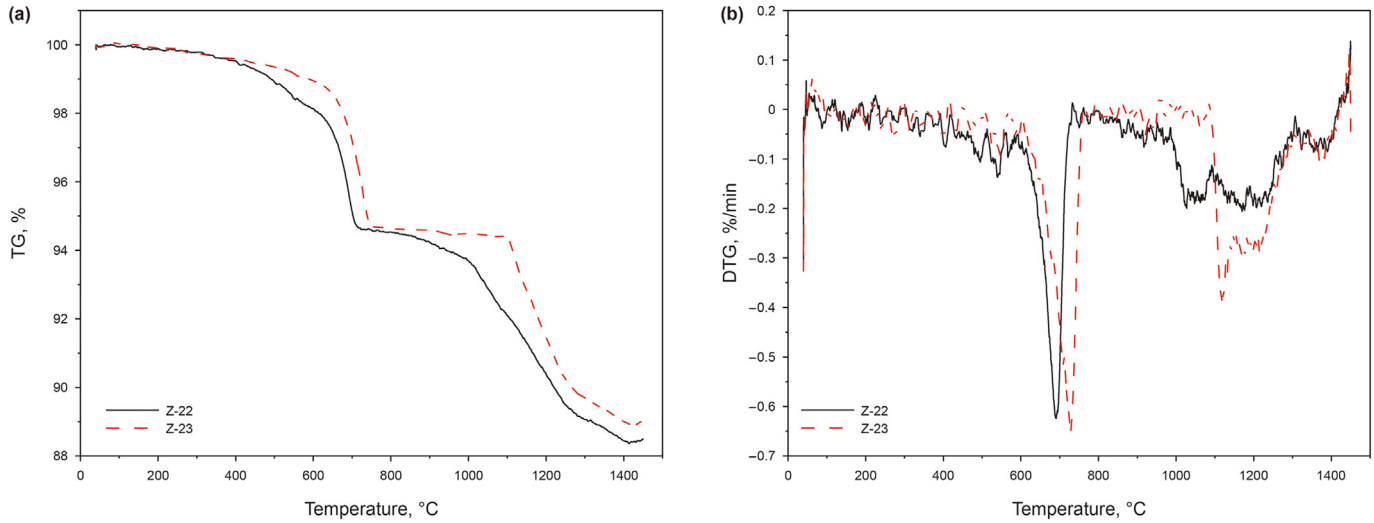

Fig. 9. TG (**a**) and DTG (**b**) curves of samples with different amounts of acid used in acid modification.

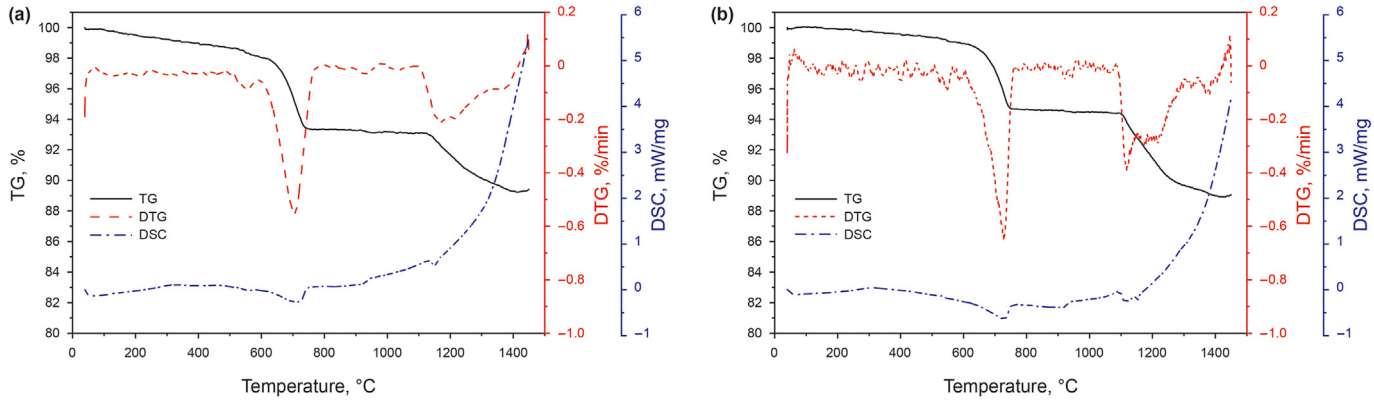

Fig. 10. Thermogravimetric analysis for the sintering process of Z-11 (**a**) and Z-23 (**b**).

process, and two obvious endothermic peaks appeared at the two weight loss peaks.

The sintering process of sample Z-23 also showed two obvious weight loss peaks. The sintering process was divided into three stages. The first weight loss peak appeared in the temperature range of 600–800 °C, and the TG curve dropped rapidly; the second obvious weight loss peak appeared in the temperature range of 1000–1400 °C. There were also two obvious endothermic peaks at the two weight loss peaks.

4. Conclusions

This study explored the possibility of preparing a ceramsite proppant from WBDC. We optimized the preparation process and prepared high-performance proppants. The parameters of the preparation process had little effect on the roundness, sphericity, and turbidity of the proppant. The other performances, including the breakage ratio, acid solubility, bulk density, and apparent density, were significantly affected by the preparation parameters. SEM and XRD results indicated that the main phases in the proppant were corundum and mullite, and the change in the preparation parameters resulted in a change in the substance content and ingredients. The TG analysis results showed that the sintering process of the proppant was divided into three stages.

Acknowledgements

The authors sincerely thank the grant funded by the Study on Comprehensive Control of Rocky Desertification and Ecological Service Function Improvement in Karst Peaks (No. 2016YFC0502402) and Fuling Shale Gas Environmental Exploration Technology of National Science and Technology Special Project (Grant No. 2016ZX05060). This work also was financially supported by the National Natural Science Foundation of China (No. 51709254), Youth Innovation Promotion Association, Chinese Academy of Sciences (No. 2020335) and Key Research and Development Program of Hubei Province, China (No. 2020BCA073). The authors would like to thank Shiyanjia Lab (www.shiyanjia.com) for the material characterization.

Appendix A. Supplementary data

Supplementary data to this article can be found online at https://doi.org/10.1016/j.petsci.2022.06.006.

References

Abd El-Kader, M., Abdou, M.I., Fadl, A.M., et al., 2020. Novel light-weight glass-ceramic proppants based on frits for hydraulic fracturing process. Ceram. Int. 46 (2), 1947–1953. https://doi.org/10.1016/j.ceramint.2019.09.173.

Chen, Y., Liu, G., Gu, Q., et al., 2019. Preparation of corundum-mullite refractories with lightweight, high strength and high thermal shock resistance. Materialia 8, 100517. https://doi.org/10.1016/j.mtla.2019.100517.

Deon, F., Regenspurg, S., Zimmermann, G., 2013. Geochemical interactions of Al_2O_3-based proppants with highly saline geothermal brines at simulated in situ temperature conditions. Geothermics 47, 53–60. https://doi.org/10.1016/j.geothermics.2013.02.003.

Han, K.-B., Graser, J., Robert, C.J., et al., 2018. Synthesis and microstructural evolution in iron oxide kaolinite based proppant as a function of reducing atmosphere, sintering conditions, and composition. Ceram. Int. 44 (8), 9976–9983. https://doi.org/10.1016/j.ceramint.2018.03.047.

Hao, C., Cheng, Y., Wang, L., et al., 2019. A novel technology for enhancing coalbed methane extraction: hydraulic cavitating assisted fracturing. J. Nat. Gas Sci. Eng. 72, 103040. https://doi.org/10.1016/j.jngse.2019.103040.

Hao, J., Ma, H., Feng, X., et al., 2018a. Low-temperature sintering of ceramic proppants by adding solid wastes. Int. J. Appl. Ceram. Technol. 15 (2), 563–568. https://doi.org/10.1111/ijac.12818.

Hao, J., Ma, H., Feng, X., et al., 2018b. Microstructure and fracture mechanism of low density ceramic proppants. Mater. Lett. 213, 92–94. https://doi.org/10.1016/j.matlet.2017.11.021.

Kao, C.-T., Tuan, W.-H., Liu, C.-Y., et al., 2018. Effect of iron oxide coloring agent on the sintering behavior of dental yttria-stabilized zirconia. Ceram. Int. 44 (5), 4689–4693. https://doi.org/10.1016/j.ceramint.2017.12.049.

Khodadadi, M., Moradi, L., Dabir, B., et al., 2020. Reuse of drill cuttings in hot mix asphalt mixture: a study on the environmental and structure performance. Construct. Build. Mater. 256, 119453. https://doi.org/10.1016/j.conbuildmat.2020.119453.

Kogbara, R.B., Ayotamuno, J.M., Onuomah, I., et al., 2016. Stabilisation/solidification and bioaugmentation treatment of petroleum drill cuttings. Appl. Geochem. 71, 1–8. https://doi.org/10.1016/j.apgeochem.2016.05.010.

Kogbara, R.B., Dumkhana, B.B., Ayotamuno, J.M., et al., 2017. Recycling stabilised/solidified drill cuttings for forage production in acidic soils. Chemosphere 184, 652–663. https://doi.org/10.1016/j.chemosphere.2017.06.042.

Leonard, S.A., Stegemann, J.A., 2010. Stabilization/solidification of petroleum drill cuttings: leaching studies. J. Hazard Mater. 174 (1), 484–491. https://doi.org/10.1016/j.jhazmat.2009.09.078.

Li, H., Lau, H.C., Huang, S., 2018. China's coalbed methane development: a review of the challenges and opportunities in subsurface and surface engineering. J. Nat. Gas Sci. Eng. 166, 621–635. https://doi.org/10.1016/j.petrol.2018.03.047.

Liu, D.-S., Wang, C.-Q., Mei, X.-D., et al., 2018. Environmental performance, mechanical and microstructure analysis of non-fired bricks containing water-based drilling cuttings of shale gas. Construct. Build. Mater. 183, 215–225. https://doi.org/10.1016/j.conbuildmat.2018.06.107.

Liu, H., Xiong, X., Li, M., et al., 2020. Fabrication and properties of mullite thermal insulation materials with in-situ synthesized mullite hollow whiskers. Ceram. Int. 46 (10), 14474–14480. https://doi.org/10.1016/j.ceramint.2020.02.245. Part A.

Liu, W., Yuan, H., Fan, Z., et al., 2021. Using water-based drilling cuttings from shale gas development to manufacture sintered bricks: a case study in the southern Sichuan Basin, China. Environ. Sci. Pollut. Res. 28 (23), 29379–29393. https://doi.org/10.1007/s11356-021-12847-4.

Liu, Z., Zhao, J., Li, Y., et al., 2016. Low-temperature sintering of bauxite-based fracturing proppants containing CaO and MnO_2 additives. Mater. Lett. 171, 300–303. https://doi.org/10.1016/j.matlet.2016.02.090.

Ma, X., Tian, Y., Zhou, Y., et al., 2016. Sintering temperature dependence of low-cost, low-density ceramic proppant with high breakage resistance. Mater. Lett. 180, 127–129. https://doi.org/10.1016/j.matlet.2016.04.080.

Nguyen, T.T., Paulsen, J.E., Landfald, B., 2021. Seafloor deposition of water-based drill cuttings generates distinctive and lengthy sediment bacterial community changes. Mar. Pollut. Bull. 164, 111987. https://doi.org/10.1016/j.marpolbul.2021.111987.

Pang, B., Wang, S., Lu, C., et al., 2019. Investigation of cuttings transport in directional and horizontal drilling wellbores injected with pulsed drilling fluid using CFD approach. Tunn. Undergr. Space Technol. 90, 183–193. https://doi.org/10.1016/j.tust.2019.05.001.

Ren, Y., Ren, Q., Wu, X., et al., 2019. Mechanism of low temperature sintered high-strength ferric-rich ceramics using bauxite tailings. Mater. Chem. Phys. 238 (1), 121929. https://doi.org/10.1016/j.matchemphys.2019.121929.

Tang, Q., Xue, G-h, Yang, S-j, et al., 2017. Study on the preparation of a free-sintered inorganic polymer-based proppant using the suspensions solidification method. J. Clean. Prod. 148 (1), 276–282. https://doi.org/10.1016/j.jclepro.2017.02.001.

Thomas, L., Tang, H., Kalyon, D.M., et al., 2019. Toward better hydraulic fracturing fluids and their application in energy production: a review of sustainable technologies and reduction of potential environmental impacts. J. Nat. Gas Sci. Eng. 173, 793–803. https://doi.org/10.1016/j.petrol.2018.09.056.

Wang, C-q, Mei, X-d, Zhang, C., et al., 2020. Mechanism study on co-processing of water-based drilling cuttings and phosphogypsum in non-autoclaved aerated concrete. Environ. Sci. Pollut. Res. 27 (18), 23364–23368. https://doi.org/10.1007/s11356-020-09029-z.

Wang, C-q, Xiong, D-m, 2021. Leaching assessment of aerated concrete made of recycled shale gas drilling cuttings: particular pollutants, physical performance and environmental characterization. J. Clean. Prod. 282 (1), 125099. https://doi.org/10.1016/j.jclepro.2020.125099.

Wang, J., Huang, Y., Zhou, F., et al., 2020. The influence of proppant breakage, embedding, and particle migration on fracture conductivity. J. Nat. Gas Sci. Eng. 193, 107385. https://doi.org/10.1016/j.petrol.2020.107385.

Wu, T., Wu, B., Zhao, S., 2013. Acid resistance of silicon-free ceramic proppant. Mater. Lett. 92, 210–212. https://doi.org/10.1016/j.matlet.2012.10.124.

Xie, X., Niu, S., Miao, Y., et al., 2019. Preparation and properties of resin coated ceramic proppants with ultra light weight and high strength from coal-series kaolin. Appl. Clay Sci. 183 (15), 105364. https://doi.org/10.1016/j.clay.2019.105364.

Xu, J., Ding, Y., Yang, L., et al., 2019. Effect of proppant deformation and embedment on fracture conductivity after fracturing fluid loss. J. Nat. Gas Sci. Eng. 71, 102986. https://doi.org/10.1016/j.jngse.2019.102986.

Yang, H., Huang, S., Zhang, Y., et al., 2020. Remediation effect of Cr(VI)-contaminated soil by secondary pyrolysis oil-based drilling cuttings ash. Chem. Eng. J. 398 (15), 125473. https://doi.org/10.1016/j.cej.2020.125473.

Yang, S., Wu, X., Han, L., et al., 2016. Migration of variable density proppant particles in hydraulic fracture in coal-bed methane reservoir. J. Nat. Gas Sci. Eng. 36, 662–668. https://doi.org/10.1016/j.jngse.2016.11.009.

Yao, S., Chang, C., Hai, K., et al., 2022. A review of experimental studies on the proppant settling in hydraulic fractures. J. Nat. Gas Sci. Eng. 208, 109211. https://doi.org/10.1016/j.petrol.2021.109211.

Zhang, G., Li, M., Gutierrez, M., 2017. Simulation of the transport and placement of multi-sized proppant in hydraulic fractures using a coupled CFD-DEM approach. Adv. Powder Technol. 28 (7), 1704–1718. https://doi.org/10.1016/j.apt.2017.04.008.